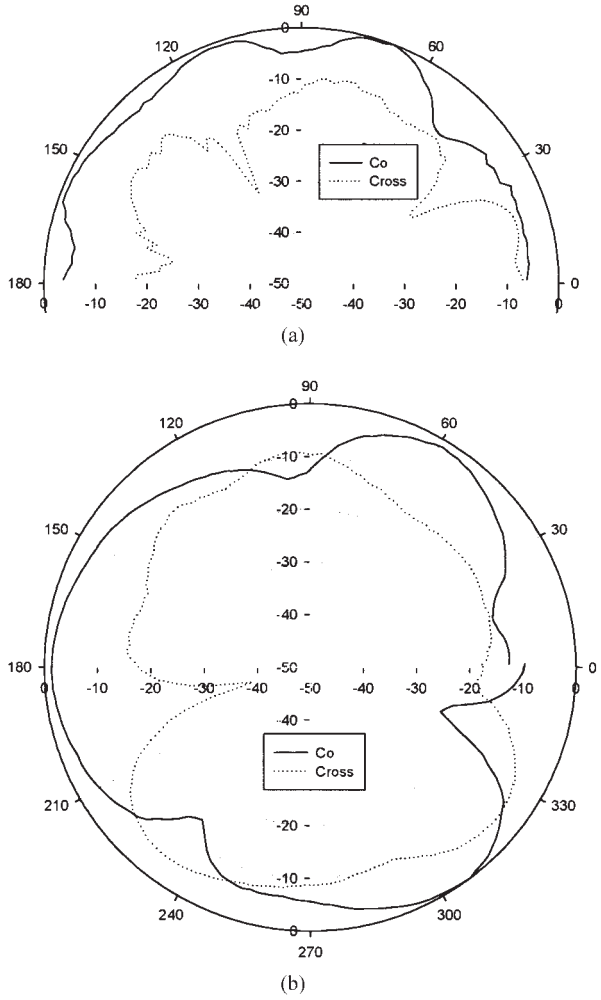

Figure 5 Radiation pattern of MDRA at 3.23 GHz: (a) elevation plane; (b) azimuth plane

presented. The return loss and radiation characteristics of the antenna have been studied. Since this proposed MDRA is capable of operating at different resonant frequencies, individual antennas operating at these frequencies can be replaced by the above MDRA and will find applications in frequency-agile systems.

ACKNOWLEDGMENT

V. Hamsakutty is thankful to UGC for providing fellowship through their Faculty Improvement Programme. A. V. Praveen Kumar is thankful to KSCSTE, Govt. of Kerala, for providing JRF. G. Bindu and A. Lonappan acknowledge CSIR for providing SRFs.

TABLE 1 Measured Results

Operating Frequency [GHz]	Measured [HPBW]		Relative Gain [dB]
	Elevation Plane	Azimuth Plane	
1.46	74°	64°	0.3
2.41	65°	50°	0.8
3.23	23°	38°	1.2

REFERENCES

1. S.A. Long, M.W. McAllister, and L.C. Shen, The resonant cylindrical dielectric cavity antenna, IEEE Trans Antennas Propagat 31 (1983), 406–412.
2. R.A. Kranenburg and S.A. Long, Microstrip transmission line excitation of dielectric resonator antennas, IEE Electron Lett 24 (1988), 1156–1157.
3. G.P. Junker, A.A. Kishk, and A.W. Glisson, Input impedance of dielectric resonator antennas excited by a coaxial probe, IEEE Trans Antennas Propagat 42 (1994), 960–965.
4. T.A. Denidni and Q. Rao, Hybrid dielectric resonator antennas with radiating slot for dual-frequency operation, IEEE Antennas Wireless Propagat Lett 3 (2004), 321–323.
5. Y. Sung, C.S. Ahn, and Y.-S. Kim, Microstrip line fed dual frequency dielectric resonator antenna, Microwave Opt Technol Lett 42 (2004), 388–390.
6. T.A. Demidhi, Q. Rao, and A.R. Sebak, Two-ring slot-fed dielectric resonator antenna for dual-frequency operation, Microwave Opt Technol Lett 44 (2005), 448–453.
7. H. Tehrani and K. Chang, A multi-frequency microstrip-fed annular slot antenna, IEEE Int APS Symp Dig, Salt Lake City, UT (2000), 632–635.
8. R.K. Raj, M. Joseph, B. Paul, and P. Mohanan, Compact planar multiband antenna for GPS, DCS, 2.4/5.8-GHz WLAN applications, IEE Electron Lett 41 (2005), 3–4.

AN EFFICIENT METHOD FOR MEASURING THE PARAMETERS OF SINGLE-MODE ANISOTROPIC SLAB WAVEGUIDES USING THE PRISM-COUPLING TECHNIQUE

Fubin Gao,[1] Guotong Du,[1] Vannadeth,[1] Ping Zhang,[2] and Fengyan Lun[2]

[1] State Key Laboratory on Integrated Opto-Electronics
College of Electronic Science and Engineering
Jilin University
Changchun 130012, P. R. China

[2] Changchun Institute of Optics
Fine Mechanics and Physics
Chinese Academy of Sciences
Changchun 130033, P. R. China

Received 9 June 2005

ABSTRACT: *An efficient method for measuring the parameters of anisotropic slab waveguides is presented in this paper. This method can be used to measure the parameters of single-mode anisotropic slab waveguides. The measured results show that the errors of the refractive indices are within* 4.2×10^{-4}. © 2005 Wiley Periodicals, Inc.

Microwave Opt Technol Lett 47: 575–580, 2005; Published online in Wiley InterScience (www.interscience.wiley.com). DOI 10.1002/mop.21234

Key words: *anisotropic slab waveguide; prism coupling technique; measurement*

1. INTRODUCTION

Recently, there has been growing interest in developing integrated optics devices in optical-communication systems. The fundamental operating principle and optimal design of optical devices such as modulators, switches, filters, and semiconductor lasers are often based on the comprehension of optical-waveguide theory. Hence, solving optical-waveguide problems is an essential way to clearly realize these devices. Most optical-waveguide devices operate in

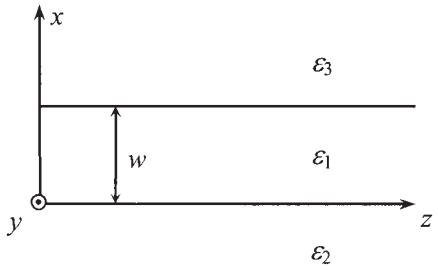

Figure 1 Geometry of an anisotropic thin-film optical waveguide

single mode, so it is very important to determine the parameters of single-mode waveguides. The prism-coupling technique has been successfully used to measure the parameters of planar waveguides using either the guided- and leaky-mode method [1–4]. But one of the disadvantages in the measurements is that the film must be thick enough to permit the propagation of at least two modes, so that two unknown parameters of isotropic dielectric waveguides can be solved from characteristic equations that are greater than or equal to the two modes. In the past ten years, the study of polymer waveguide devices has developed rapidly. Because the stability of polymer materials is not as good as that of inorganic materials, it is necessary to measure the waveguide parameters expediently and effectively for this research. In addition, the birefringence property is an important parameter for polymer waveguides. By measuring the difference of the extraordinary and ordinary refractive indices, the optical anisotropy of flexible polyimide thin films was characterized [5]. To obtain electro-optic confidents as high as possible, polymer waveguides of electro-optic modulators must be poled sufficiently and by measuring the difference of extraordinary and ordinary refractive indices, its electro-optic property can be characterized [6]. For the 2nd-order nonlinear polymer, its nonlinear optics property [7, 8] can also be characterized by measuring the difference of the extraordinary and ordinary refractive indices. Nonlinear prism coupling was also used to characteristic the optical nonlinearity of the waveguides of the conjugated polymer MEH-PPV [9]. On the other hand, polarization dependence is a main subject in the study on single-mode wavelength-division multiplexers/demultiplexers with arrayed waveguide grating (AWG). Therefore, measuring anisotropic dielectric-waveguide parameters, especially of single-mode waveguides, is very important for studying many optical waveguide devices. But the guided- or leaky-mode methods have been applied to measure the parameters of isotropic dielectric waveguides [1–4].

Based on the fact that there are both guided and leaky modes in a waveguide, we present a guided- and leaky-mode method for measuring anisotropic dielectric-waveguide parameters in this paper. This method can be applied to measuring single-mode waveguide parameters because of the sequential measurement of the guided and leaky modes' effective indices. Therefore, this method can be used not only as an efficient means for characterizing the property of electro-optic waveguide devices and polarization dependence of AWG and multimode interference (MMI) devices, but also can supply the necessary parameters for the optimization of optical waveguide devices.

2. CHARACTERISTIC EQUATIONS OF ANISOTROPIC SLAB WAVEGUIDES

As shown in Figure 1, the waveguide treated here is a 2D structure consisting of three layers: the substrate, the film, and the top layer. The materials are all assumed lossless. The direction of wave propagation is parallel to the z-axis and the structure is uniform in the y direction. The thickness of the film is w.

Dielectric tensors of anisotropic materials filling three regions are all of the following form [10]:

$$[\tilde{\varepsilon}] = \varepsilon_0[\varepsilon] = \varepsilon_0\begin{bmatrix} \varepsilon_{xx} & \varepsilon_{xy} & \varepsilon_{xz} \\ \varepsilon_{xy}^* & \varepsilon_{yy} & \varepsilon_{yz} \\ \varepsilon_{xz}^* & \varepsilon_{yz}^* & \varepsilon_{zz} \end{bmatrix}, \quad (1)$$

where ε_0 is the permittivity of vacuum, and $[\varepsilon]$ is the relative dielectric tensors.

In the principal coordinate system, only diagonal terms of $[\varepsilon]$ are nonzero, and $[\varepsilon]$ is given by

$$[\varepsilon] = \begin{bmatrix} \varepsilon_{xx} & 0 & 0 \\ 0 & \varepsilon_{yy} & 0 \\ 0 & 0 & \varepsilon_{zz} \end{bmatrix}. \quad (2)$$

Under this condition, the anisotropic characteristic equation for the TE mode is shown as follows

$$\kappa_{1\mathrm{TE}} w = m_{\mathrm{TE}}\pi + \phi_{12\mathrm{TE}} + \phi_{13\mathrm{TE}}, \quad (m_{\mathrm{TE}} = 0, 1, 2, \cdots\cdots), \quad (3)$$

where m_{TE} is the mode-order number for the TE mode, $\phi_{12\mathrm{TE}}$ and $\phi_{13\mathrm{TE}}$ are the phase shifts occurring at the 1–2 and 1–3 interfaces, respectively, $\kappa_{1\mathrm{TE}}$ is the propagation constant in the x direction and expressed in terms of a propagation constant in the z direction β_{TE}, and the free-space propagation constant k_0 is given by

$$\kappa_{1\mathrm{TE}}^2 = k_0^2\varepsilon_{1yy} - \beta_{m\mathrm{TE}}^2. \quad (4)$$

In the case of $\varepsilon > \varepsilon_2 \geq \varepsilon_3$, the expressions of $\phi_{12\mathrm{TE}}$ and $\phi_{13\mathrm{TE}}$ depend on the value of the angle of incidence θ_1 and the TE-polarized light propagating in the film.

If $\theta_1 > \theta_{12c}$ and θ_{13c} (θ_{12c} and θ_{13c} are the critical angle at the 1–2 and 1–3 interfaces, respectively), the ray suffers total internal reflection at each interface, as shown in Figure 2(a). The result is a series of discrete guided modes.

In the region $\theta_{12c} > \theta_1 > \theta_{13c}$, the ray suffers total internal reflection at the 1–3 interface and partial internal reflection at the 1–2 interface, as shown in Figure 2(b). This leads to a series of discrete modes called leaky waves in the substrate radiation-mode regime.

Finally, when $\theta_1 < \theta_{13c}$, the ray suffers partial internal reflection at both interfaces, as shown in Figure 2(c). We obtain a series of discrete modes, which lead to leaky waves in the cladding radiation-mode regime. These modes leak both into the substrate and into the cladding. Therefore, the phase shifts at the 1–2 and 1–3 interfaces are respectively given by

$$\phi_{12\mathrm{TE}} = \begin{cases} \tan^{-1}(p_{\mathrm{TE}}/\kappa_{1\mathrm{TE}}), & \theta_1 \geq \theta_{12c} \\ \pi/2, & \theta_1 < \theta_{12c}, \end{cases} \quad (5)$$

$$\phi_{13\mathrm{TE}} = \begin{cases} \tan^{-1}(q_{\mathrm{TE}}/\kappa_{1\mathrm{TE}}), & \theta_1 \geq \theta_{13c} \\ \pi/2, & \theta_1 < \theta_{13c}, \end{cases} \quad (6)$$

$$p_{\mathrm{TE}}^2 = \beta_{m\mathrm{TE}}^2 - k_0^2\varepsilon_{2yy}, \quad (7)$$

$$q_{\mathrm{TE}}^2 = \beta_{m\mathrm{TE}}^2 - k_0^2\varepsilon_{3yy}, \quad (8)$$

Similarly, the anisotropic characteristic equation for the TM mode is shown as follows:

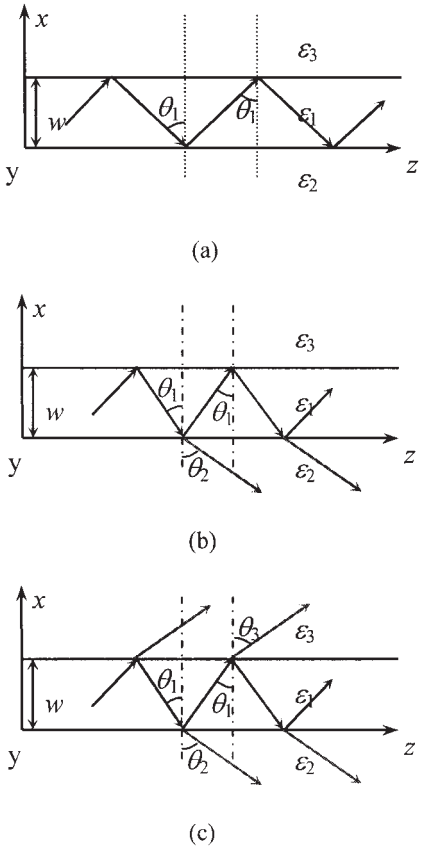

Figure 2 Zigzag path of a ray as a (a) guided mode in the real waveguide; (b) leaky mode in the one-sided leaky waveguide; (c) leaky mode in the two-sided leaky waveguide

$$\kappa_{1\mathrm{TM}} w = m_{\mathrm{TM}}\pi + \phi_{12\mathrm{TM}} + \phi_{13\mathrm{TM}}, \quad (m_{\mathrm{TM}} = 0, 1, 2, \cdots\cdots), \tag{9}$$

$$\kappa_{1\mathrm{TM}}^2 = \frac{\varepsilon_{1zz}}{\varepsilon_{1xx}}(k_0^2\varepsilon_{1xx} - \beta_{m\mathrm{TM}}^2), \tag{10}$$

In the case of $\varepsilon_1 > \varepsilon_2 \geq \varepsilon_3$, the expressions of $\phi_{12\mathrm{TM}}$ and $\phi_{13\mathrm{TM}}$ depend on the value of the angle of incidence θ_1 of the TM-polarized light propagating in the film.

We consider the phase shift occurring at the 1–2 interface. First, if $\theta_1 > \theta_{12c}$, the ray suffers total internal reflection, and $\phi_{12\mathrm{TM}}$ is the phase shifts of total internal reflection. Second, in the region $\theta_{12c} > \theta_1 > \theta_{12p}$ (θ_{12p} is Brewster's angle at the 1–2 interface), the ray suffers partial internal reflection, and $\phi_{12\mathrm{TM}} = 0$ is derived from Fresnel formulae [11]. Third, when $\theta_1 < \theta_{12p}$, the ray also suffers partial internal reflection, but $\phi_{12\mathrm{TM}} = \pi/2$ derived from Fresnel formulae [11], too.

Likewise, we can obtain the phase shift occurring at the 1–3 interface, which is same as that at the 1–2 interface replacing θ_{12c} and θ_{12p} by θ_{13c} and θ_{13p}, respectively. Therefore, the phase shifts at the 1–2 and 1–3 interfaces are respectively given by

$$\phi_{12\mathrm{TM}} = \begin{cases} \tan^{-1}\left(\dfrac{\varepsilon_{1zz}}{\varepsilon_{2zz}}\dfrac{p_{\mathrm{TM}}}{\kappa_{1\mathrm{TM}}}\right), & \theta_1 \geq 0 \\ 0, & \theta_{12p} < \theta_1 < \theta_{12c}, \\ \dfrac{\pi}{2}, & \theta_1 < \theta_{12p} \end{cases} \tag{11}$$

$$\phi_{13\mathrm{TM}} = \begin{cases} \tan^{-1}\left(\dfrac{\varepsilon_{1zz}}{\varepsilon_{3zz}}\dfrac{q_{\mathrm{TM}}}{\kappa_{1\mathrm{TM}}}\right), & \theta_1 \geq \theta_{13c} \\ 0, & \theta_{13p} < \theta_1 < \theta_{13c}, \\ \dfrac{\pi}{2}, & \theta_1 < \theta_{13p} \end{cases} \tag{12}$$

$$p_{\mathrm{TM}}^2 = \frac{\varepsilon_{2zz}}{\varepsilon_{2xx}}(\beta_{m\mathrm{TM}}^2 - k_0^2\varepsilon_{2xx}), \tag{13}$$

$$q_{\mathrm{TM}}^2 = \frac{\varepsilon_{3zz}}{\varepsilon_{3xx}}(\beta_{m\mathrm{TM}}^2 - k_0^2\varepsilon_{3xx}). \tag{14}$$

3. WAVEGUIDE MODEL AND PARAMETERS

The waveguide studied here is made up of the isotropic substrate, the isotropic to layer, and the uniaxial-guided layer. The terms of dielectric tensor of the substrate are

$$\varepsilon_{2xx} = \varepsilon_{2yy} = \varepsilon_{2zz} = n_b^2, \tag{15}$$

and the terms of dielectric tensor of the top layer are

$$\varepsilon_{3xx} = \varepsilon_{3yy} = \varepsilon_{3zz} = n_c^2, \tag{16}$$

where n_b and n_c are the substrate and the top layer refractive indices, respectively.

The refractive-index ellipsoid of the uniaxial-guided layer is a uniaxial ellipsoid, as shown in Figure 3(a). Hence, the terms of dielectric tensor are

$$\varepsilon_{1xx} = n_e^2, \quad \varepsilon_{1yy} = \varepsilon_{1zz} = n_o^2, \tag{17}$$

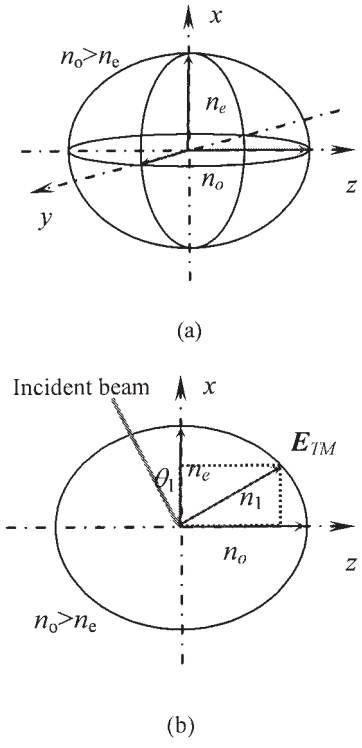

Figure 3 (a) The refractive-index ellipsoid of the uniaxial-guided layer; (b) the refractive index ellipse in the x–z plane

where n_e and n_o are called the extraordinary refractive index parallel to the x-axis and the ordinary refractive index in the y–z plane, respectively.

The propagation constants for TE and TM modes in z direction are expressed by

$$\beta_{m\mathrm{TE}} = k_0 N_{m\mathrm{TE}}, \quad \beta_{m\mathrm{TM}} = k_0 N_{m\mathrm{TM}}, \tag{18}$$

where $N_{m\mathrm{TE}}$ and $N_{m\mathrm{TM}}$ are TE and TM modes effective refractive indices, respectively.

Substituting Eqs. (15)–(18) into Eqs. (3)–(4), we obtain

$$wk_0\sqrt{n_o^2 - N_{m\mathrm{TE}}^2} = m_{\mathrm{TE}}\pi + \phi_{12\mathrm{TE}} + \phi_{13\mathrm{TE}}, \quad (m_{\mathrm{TE}} = 0, 1, 2, \cdots\cdots), \tag{19}$$

$$\phi_{12\mathrm{TE}} = \begin{cases} \tan^{-1}\dfrac{\sqrt{N_{m\mathrm{TE}}^2 - n_b^2}}{\sqrt{n_o^2 - N_{m\mathrm{TE}}^2}}, & N_{m\mathrm{TE}} \geq n_b \\ \pi/2, & N_{m\mathrm{TE}} < n_b \end{cases}, \tag{20}$$

$$\phi_{13\mathrm{TE}} = \begin{cases} \tan^{-1}\dfrac{\sqrt{N_{m\mathrm{TE}}^2 - n_c^2}}{\sqrt{n_o^2 - N_{m\mathrm{TE}}^2}}, & N_{m\mathrm{TE}} \geq n_c \\ \pi/2, & N_{m\mathrm{TE}} < n_c \end{cases}, \tag{21}$$

$$wk_0\frac{n_o}{n_e}\sqrt{n_e^2 - N_{m\mathrm{TM}}^2} = m_{\mathrm{TM}}\pi + \phi_{12\mathrm{TM}} + \phi_{13\mathrm{TM}}, \quad (m_{\mathrm{TM}} = 0, 1, 2, \cdots\cdots), \tag{22}$$

$$\phi_{12\mathrm{TM}} = \begin{cases} \tan^{-1}\left(\dfrac{n_o n_e}{n_b^2}\dfrac{\sqrt{N_{m\mathrm{TM}}^2 - n_b^2}}{\sqrt{n_e^2 - N_{m\mathrm{TM}}^2}}\right), & N_{m\mathrm{TM}} \geq n_b \\ 0, & N_{12p} \leq N_{m\mathrm{TM}} < n_b \\ \dfrac{\pi}{2}, & N_{m\mathrm{TM}} < N_{12p} \end{cases}, \tag{23}$$

$$\phi_{13\mathrm{TM}} = \begin{cases} \tan^{-1}\left(\dfrac{n_o n_e}{n_c^2}\dfrac{\sqrt{N_{m\mathrm{TM}}^2 - n_c^2}}{\sqrt{n_e^2 - N_{m\mathrm{TM}}^2}}\right), & N_{m\mathrm{TM}} \geq n_c \\ 0, & N_{13p} \leq N_{m\mathrm{TM}} < n_c \\ \dfrac{\pi}{2}, & N_{m\mathrm{TM}} < N_{13p} \end{cases}, \tag{24}$$

where N_{12p} and N_{13p} are the TM mode effective refractive indices related the Brewster's angles θ_{12p} and θ_{13p}, respectively.

For the TM-polarized light, the index ellipse in the incident plant is shown in Figure 3(b), and its equation is given by

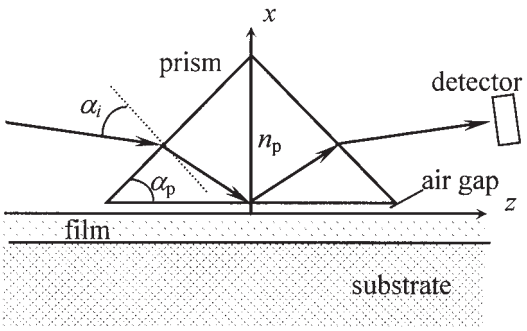

Figure 4 Schematic diagram of the prism coupler

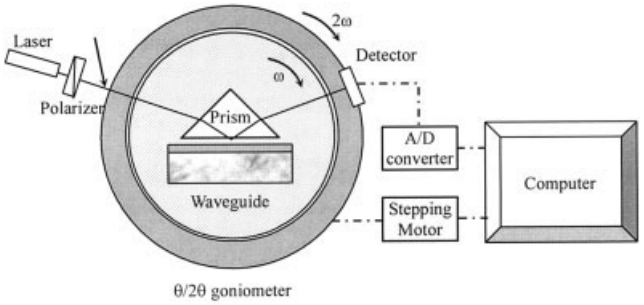

Figure 5 Schematic diagram of the synchronous measurement system

$$\frac{n_1^2\cos^2\theta_1}{n_o^2} + \frac{n_1^2\sin^2\theta_1}{n_e^2} = 1. \tag{25}$$

The real refractive indices n_{12p} and n_{13p} for $\theta_1 = \theta_{12p}$ and $\theta_1 = \theta_{13p}$ can be derived from Eq. (25) and Brewster's formula, respectively, and expressed as follows

$$n_{12p} = \frac{2n_e n_o n_b}{\sqrt{2n_o(n_o n_b^2 + \sqrt{n_o^2 n_e^4 - 2n_o^2 n_e^2 n_b^2 + n_o^2 n_b^4 + 4n_b^2 n_e^4 - n_o n_e^2})}}, \tag{26}$$

$$n_{13p} = \frac{2n_e n_o n_c}{\sqrt{2n_o(n_o n_c^2 + \sqrt{n_o^2 n_e^4 - 2n_o^2 n_e^2 n_c^2 + n_o^2 n_c^4 + 4n_c^2 n_e^4 - n_o n_e^2})}}, \tag{27}$$

so that

$$N_{12p} = n_{12p}\sin\left(\tan^{-1}\frac{n_b}{n_{12p}}\right) = \frac{n_{12p}n_b}{\sqrt{n_{12p}^2 + n_b^2}}, \tag{28}$$

$$N_{13p} = n_{13p}\sin\left(\tan^{-1}\frac{n_c}{n_{13p}}\right) = \frac{n_{13p}n_c}{\sqrt{n_{13p}^2 + n_c^2}}. \tag{29}$$

4. MEASUREMENT AND DATA TREATMENT

The mode-effective refractive indices of waveguides can be measured by using the prism-coupling technique [1]. The prism coupler is shown schematically in Figure 4. The measurement setup in our experiment is shown schematically in Figure 5. The measurements are made using the polarized laser beam from a semiconductor laser operating at a wavelength λ of 650 nm. The output beam is detected by a silicon solar-cell detector.

The prism coupler is mounted on a goniometric table driven by a stepping motor. While the table is rotating at an angular velocity ω, the detector can be rotating at the angular velocity 2ω in the same direction, so that the detector is always located in the direction of the output beam from the prism, and the signal of the photocurrent varying with the incidence angle α_i can be detected in real time. After being amplified by an artificial circuit, the analog signal is transformed to the digital signal by an A/D converter. The digital-signal data are collected by a computer. According to the curves of the output light intensity varying with α_i drawn by the computer, the excitation of the guided and leaky modes can be identified by the negative peaks, so that the synchronous angles α_m related with the mode-order number m are determined. The mode-effective refractive index N_m can be then calculated as follows:

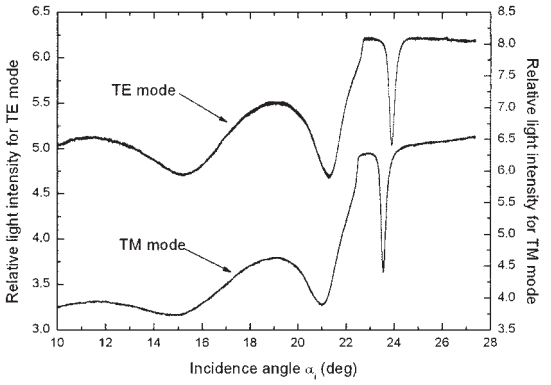

(a)

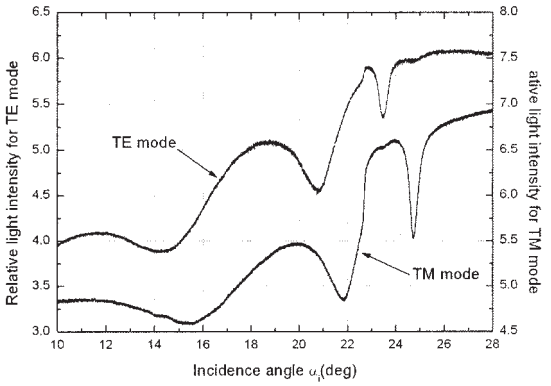

(b)

Figure 6 Curves of relative light intensity while varying the incidence angle (a) before poling and (b) after poling

$$N_m = \sin\alpha_m \cos\alpha_p + \sin\alpha_p \sqrt{n_p^2 - \sin^2\alpha_m}, \quad (m = 0, 1, 2, \ldots), \tag{30}$$

where n_p and α_p are the prism refractive index and angle, respectively.

If the numbers of observed $N_{m\mathrm{TE}}$ and $n_{m\mathrm{TM}}$ are M_{TE} and M_{TM}, respectively, Eqs. (19) and (22) form an equation system involving $M_{\mathrm{TE}} + M_{\mathrm{TM}}$ transcendental equations about three unknowns, n_c, n_o, and w.

To find the unknown parameters n_e, n_o, and w, the objective function is defined as follows:

$$S = \left[\sum_{m\mathrm{TE}=0}^{M_{m\mathrm{TE}}-1} (\Delta N_{m\mathrm{TE}})^2 + \sum_{m\mathrm{TE}=0}^{M_{m\mathrm{TM}}-1} (\Delta N_{m\mathrm{TM}})^2 \right]^{1/2} \Big/ (M_{m\mathrm{TE}} + M_{m\mathrm{TM}}), \tag{31}$$

$$\Delta N_{m\mathrm{TE}} = N_{m\mathrm{TE}} - N_{m\mathrm{TE0}}(n_e, n_o, w), \quad \Delta N_{m\mathrm{TM}} = N_{m\mathrm{TM}} - N_{m\mathrm{TM0}}(n_e, n_o, w), \tag{32}$$

where $N_{m\mathrm{TE0}}(n_e, n_o, w)$ and $N_{m\mathrm{TM0}}(n_e, n_o, w)$ are the theoretical value of $N_{m\mathrm{TE}}$ and $N_{m\mathrm{TM}}$. For the given values of n_e, n_o, and w, $N_{m\mathrm{TE0}}$ can be found numerically from Eqs. (19) and (22) with a computer.

We can adjust the unknown parameters n_e, n_o, and w until S approaches minimum as closely as possible. We regard the parameters n_{e0}, n_{o0}, and w_0, for which S is equal to the minimum $S_{\min}$, as the measured values of n_e, n_o, and w. The measured error in $S_{\min}$.

5. RESULTS AND DISCUSSION

A sample of slab optical waveguides was fabricated by spin-coating doped DR1/PMMA polymer solution on a glass-substrate slide at a certain rotation speed. Then it was solidified at 60°C for 24 h in vacuum.

The DR1 polymer waveguide sample was measured and the curves of the relative light-intensity output from the prism varying with the incidence angle are shown in Figure 6. In the measurement, n_p and α_p of a symmetrical glass prism are 1.79785° and 44.9944°, respectively. The refractive indices of the substrate and the top layer (air) are 1.51572 and 1.0000, respectively. There are one sharp negative peak of the guided mode and two (not sharper) negative peaks of the leaky modes for each polarization. Therefore, we obtained six measured values of the synchronous angles for both TE and TM modes, as shown in Figure 6(a).

After that, the sample was corona-poled at 92° for 60 min. The poled waveguide sample was measured and the curves of relative light intensity output from the prism varying with the incidence angle are shown in Figure 6(b).

The polymer waveguide parameters before and after corona poling have been calculated using our MATLAB programs and both results are listed in Table 1.

For the single-mode waveguide, we can only obtain two measured values of the effective refractive indices of the guided modes corresponding to the TE and TM modes, respectively, so that we

TABLE 1 Measured Data and Calculated Results for the Sample of DR1/PMMA Polymer Waveguide

(a) Before Poling					(b) After Poling				
m_{TE}	$a_{m\mathrm{TE}}$ [°]	$N_{m\mathrm{TE}}$	$N_{m\mathrm{TE0}}$	$\Delta N_{m\mathrm{TE}}$	m_{TE}	$a_{m\mathrm{TE}}$ [°]	$N_{m\mathrm{TE}}$	$N_{m\mathrm{TE0}}$	$\Delta N_{m\mathrm{TE}}$
0	23.8716	1.52471	1.52382	8.9×10^{-4}	0	23.4718	1.52128	1.52100	2.2×10^{-4}
1	21.2265	1.50114	1.50092	2.2×10^{-4}	1	20.7622	1.49688	1.49556	13.2×10^{-4}
2	15.2968	1.44395	1.44515	-12×10^{-4}	2	14.3011	1.43378	1.43525	-14.7×10^{-4}
m_{TM}	$a_{m\mathrm{TM}}$ [°]	$N_{m\mathrm{TM}}$	$N_{m\mathrm{TM0}}$	$\Delta N_{m\mathrm{TM}}$	m_{TM}	$a_{m\mathrm{TM}}$ [°]	$N_{m\mathrm{TM}}$	$N_{m\mathrm{TM0}}$	$\Delta N_{m\mathrm{TM}}$
0	23.5490	1.52190	1.52317	-12.6×10^{-4}	0	24.7363	1.53215	1.53305	-9.0×10^{-4}
1	20.9484	1.49859	1.49859	0.0×10^{-4}	1	21.8460	1.50677	1.50736	-5.9×10^{-4}
2	14.9039	1.43996	1.43911	8.4×10^{-4}	2	15.2224	1.44320	1.44214	10.6×10^{-4}
$n_{o0} = 1.53148$		$w_0 = 1.5107\ \mu\mathrm{m}$			$n_{o0} = 1.52860$		$w_o = 1.4521\ \mu\mathrm{m}$		
$n_{e0} = 1.53124$		$S_{\min} = 3.6 \times 10^{-4}$			$n_{e0} = 1.54309$		$S_{\min} = 4.2 \times 10^{-4}$		

cannot solve three unknown parameters from two characterization equations. However, by using our method, two guided-mode effective refractive indices and four leaky-mode effective refractive indices can be obtained, so that the parameters of the single-mode waveguide can be calculated from six characteristic equations.

According to the calculated results, the measured values of n_e and n_o before poling is equal in the range of the measurement error. This indicates that the DR1 polymer waveguide is approximately an isotropy waveguide. After poling, n_e is greater than n_o, which indicates that the DR1 polymer waveguide is a uniaxial anisotropy waveguide. In fact, the DR1/PMMA polymer is just used as electro-optic polymer waveguide material, and the waveguide can have the electro-optic characteristic via corona poling.

With regard to the error problem, one of the causes of errors is the determination of the reference angle, equivalent to the goniometer table position, where the incident laser beam is perpendicular to the incidence face of the prism. In our measurements, we determine the reference angle by manually adjusting the table so that the laser beam reflected from the incidence face of the prism returns to the incidence direction. Due to this manual adjustment and visual identification, the main random error occurs. Another error originates from the determination of the position of the negative peak, especially the peak related to the leaky modes. Both the above errors are artificial errors. In the computer-program solving process, we assume that the computing error of independent variables is equal to 1×10^{-5} and the computing error of the function of the mode characterized equation is equal to 1×10^{-5} as well. In practice, the synthesis error is about equal to or less than 4.2×10^{-4}, so we can consider that the artificial error is the main origin and the computing errors can be neglected.

6. CONCLUSION

By using our sequential measurement system, the guided- and leaky-mode curves of anisotropic dielectric waveguides have been measured. The single-mode waveguide parameters have been solved from the transcendental equation system formed by the guided- and leaky-mode equations. Although the measurement error is greater than that obtained only by guided-mode equations due to the leaky modes, the measurement parameters of single-mode anisotropic waveguides are sufficient for the design of optical-waveguide devices.

ACKNOWLEDGMENT

This work was financially supported by the National Natural Science Foundation of China under project no. 60274041.

REFERENCES

1. R. Ulrich and R. Torge, Measurement of film parameters with a prism coupler, Appl Optics 12 (2001), 2901–2908.
2. A.C. Adams, D.P. Schinke, and C.D. Capio, An evaluation of the prism coupler for measuring the thichness and refractive index of dielectric films on silicon substrates, J Electrochem Soc 126 (1979), 1539–1543.
3. T.W. Hou and C.J. Mogab, Plasma silicon oxide films on garnet substrates: measurement of their thickness and refractive index by the prism coupling technique, Appl Optics 20 (1981), 3184–3188.
4. Tie-Nan Ding and Elsa Garmire, Measuring refractive index and thickness of thin films: a new technique, Appl Optics 22 (1983), 3177–3181.
5. B. Li, T. He, M. Ding, P. Zhang, F. Gao, and F. Jin, Optical anisotropy of flexible polyimide thin films, J Mater Res 13 (1998), 1368–1372.
6. F. Gao, F. Jin, and R. Xing, A guided-mode method for measuring electro-optic coefficients of poled polymer waveguides, SPIE 2987 (1996), 304–308.
7. F. Gao, P. Zhang, F. Jin, R. Xing, S. Wang, C. Ye, and Z. Feng, Fabrication and characterization of corona-poled NPP polymer waveguides for second harmonic generation, SPIE 3556 (1998), 117–121.
8. R. Xing, F. Jin, and F. Gao, Stable second-order nonlinear optical waveguide with interpenetrating polymer network, SPIE 2987 (1996), 221–225.
9. K. Koynov, N. Goutev, Fitrilawati, A. Bahtiar, A. Best, and C. Bubeck, Nonlinear prism couling of waveguides of the conjugated polymer MEH-PPV and their figures of merit for all-optical switching, J Optics Soc Am B 19 (2002), 895–901.
10. S. Yamamoto, Y. Koyamada, and T. Makimoto, Normal-mode analysis of anisotropic and gyrotropic thin-film waveguides for integrated optics, J Appl Phys 43 (1972), 5090–5097.
11. M. Born and E. Wolf, Principles of optics, Pergamon, New York, 1965.

CPW-FED TRIANGULAR MONOPOLE ANTENNA FOR ULTRA-WIDEBAND OPERATION

Wen-Chung Liu[1] and Ping-Chi Kao[2]

[1] Department of Aeronautical Engineering
National Formosa University
64, Wenhua Road
Huwei, Yunlin 632
Taiwan, Republic of China

[2] Institute of Electro-Optical and Materials Science
National Formosa University
64, Wenhua Road
Huwei, Yunlin 632
Taiwan, Republic of China

Received 8 June 2005

ABSTRACT: *A novel ultra-wideband design of a single-layer coplanar waveguide (CPW)-fed triangular planar monopole antenna is proposed. The proposed antenna, which includes two notched ground planes only 24 mm in width and 31 mm in height, experimentally reaches a measured −10-dB impedance bandwidth of 9.8 GHz (from 3.05 to 12.85 GHz), covering the WPAN standard. Good monopolelike radiation patterns and antenna gains are also obtained.* © 2005 Wiley Periodicals, Inc. Microwave Opt Technol Lett 47: 580–582, 2005; Published online in Wiley InterScience (www.interscience.wiley.com). DOI 10.1002/mop.21235

Key words: *coplanar waveguide (CPW)-fed; monopole antenna; ultra-wideband*

1. INTRODUCTION

Recently, interest in ultra-wideband (UWB) communication systems, such as the new wireless personal area network (WPAN) covering 3.1–10.6 GHz, has rapidly increased due to their many advantages, including low-spectral-density radiated power and the potential for accommodating higher data rates. However, one of the most challenging of the main issues involved in designing UWB systems is to design a wideband antenna with compact size and easy integration with communication modules. For the available designs, the stepped- and slotted-patch antenna, the slotted antenna printed on a low-temperature co-fired ceramic substrate, the coplanar waveguide (CPW)-fed triangular monopole with L-shaped grounds, and the CPW-fed slotted monopole with parasitic elements, reported in [1–4], respectively, are all capable of UWB operation; however, they are either complex in antenna shape or large in antenna size.